Electronic Supplementary Information

Cobalt oxide-polypyrrole nanocomposite as efficient and stable electrode material for electrocatalytic water oxidation

Daniela V. Morales,[a,b] Catalina N. Astudillo,[a] Veronica Anastasoaie,[a,c] Baptiste Dautreppe,[a] Bruno F. Urbano,[d] Bernabé L. Rivas,[d] Chantal Gondran,[a] Dmitry Aldakov,[e] Benoit Chovelon,[f,g] Dominique André,[f] Jean-Luc Putaux,[h] Christine Lancelon-Pin,[h] Selim Sirach,[a] Eleonora-Mihaela Ungureanu,[c] Cyrille Costentin,[a,i] Marie-Noëlle Collomb[a] and Jérôme Fortage*[a]*

[a]Univ. Grenoble Alpes, CNRS, DCM, 38000 Grenoble, France. E-mail: jerome.fortage@univ-grenoble-alpes.fr; marie-noëlle.collomb@univ-grenoble-alpes.fr

[b]Department of Environmental Chemistry, Faculty of Sciences, Universidad Católica de la Santísima Concepción, Concepción, Chile

[c]Department of Inorganic Chemistry, Physical Chemistry and Electrochemistry, Faculty of Applied Chemistry and Materials Science, University Politehnica of Bucharest, Splaiul Independentei, 313, 060042 Bucharest, Romania

[d]Polymer Department, Faculty of Chemistry, University of Concepción, Concepción, Chile

[e]Univ. Grenoble Alpes, CNRS, CEA, IRIG, SyMMES, 38000 Grenoble, France

[f]Unit Nutritional and Hormonal Biochemistry - Institut de biologie et de pathologie, CHU de Grenoble Site Nord, F-38041, Grenoble, France

[g]Univ. Grenoble Alpes, DPM UMR 5063, F-38041 Grenoble, France

[h]Univ. Grenoble Alpes, CNRS, CERMAV, F-38000 Grenoble, France

[i]Université de Paris, 75013 Paris, France

1. Chemicals and Reagents. The monomer (3-pyrrole-1-yl-propyl)-triethylammonium tetrafluoroborate, denoted PN^+ (Scheme S1), was prepared as previously reported.[1] Cobalt(II) sulfate hexahydrate ($CoSO_4 \bullet 6H_2O$, 99% Acros), sodium oxalate ($Na_2C_2O_4$, 99% Prolabo), boric acid (H_3BO_3, 99.5% Normapur), acetonitrile (Fisher, HPLC grade), sodium sulfate (Na_2SO_4, 99% Laurylab), sodium hydroxide (NaOH, 99% Laurylab), potassium hydroxide (KOH, ≥85% Prolabo) and tetra-*n*-butylammonium perchlorate ($[Bu_4N]ClO_4$, Fluka puriss) were purchased from commercial suppliers. All reagents and solvents were used as received. Distilled water was obtained from an Elga water purification system (milli-Q system, Purelab option, 15.0 MΩ.cm, 24 °C).

Scheme S1. Pyrrole-based monomer (PN^+)

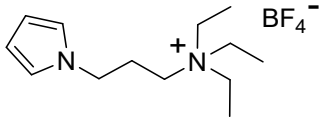

2. Electrochemistry. The electrochemical experiments were performed using a conventional three-electrode system. Electropolymerization of poly(pyrrole-alkylammonium) film (denoted PPN^+) were performed in acetonitrile in a dry-glove box using an EGG PAR Model 173 potensiostat under argon atmosphere at room temperature. Electrodeposition of Co^0, electrooxidation into CoO_x and electroanalytical experiments were performed using a CHI 660B Electrochemical analyser (CH Instruments) in aqueous solution. Electrodeposition of Co^0 was performed in a solution purged with argon while the electrooxidation into CoO_x was performed under air atmosphere. Potentials were referred to Ag/AgCl (3 M KCl in water) or $Ag/AgNO_3$ (10 mM $AgNO_3$ in CH_3CN + 0.1 M $[Bu_4N]ClO_4$) references electrodes in aqueous and acetonitrile solutions, respectively. Potentials referred to the Ag/AgCl (3 M KCl) system can be converted to the reversible hydrogen electrode (RHE)[2] according to the Nernst equation S1:

$$E_{RHE} = E_{Ag/AgCl} + 0.059 \times pH + E^{o}_{Ag/AgCl} \quad \text{(S1)}$$

where $E^{o}_{Ag/AgCl}$ = 0.199 V *vs* NHE at 25°C and NHE is the normal hydrogen electrode.

Potentials referred to the $Ag/AgNO_3$ reference electrode can be converted to Ag/AgCl (3 M KCl) by adding 330 mV.

For analytical experiments, the films of PPN^+ and Co^0 were electrodeposited on glassy carbon working electrodes (denoted C, 3 mm in diameter corresponding to a surface of 0.071 cm^2). These electrodes were polished with 1 µm diamond paste before coating. For microscopy characterizations, the films of PPN^+ and Co^0 were electrodeposited on indium tin oxide-coated glass electrodes (ITO, surface of 1.0 cm^2, 70 Ohms (Solems)). For X-ray photoelectron spectroscopy (XPS) measurements, PPN^+ and Co^0 were electrodeposited on carbon pellets (denoted C_{pel}, 6 mm in diameter corresponding to a surface of 0.283 cm^2, (Origalys)). The modified carbon pellets are easily unscrewed from the electrode holder in order to introduce the C_{pel}/PPN^+-CoO_x and C_{pel}/CoO_x samples into the vacuum chamber of the XPS

spectrometer. In order to increase the stability of the PPN^+-CoO_x composite material at the electrode surface under prolonged electrolysis at 1.2 V *vs* Ag/AgCl, films of PPN^+ were also deposited onto Toray carbon paper (denoted C_{pap}, surface of 2.4 cm^2, from E-TEK, TGP-H-120, 0.37 mm of thickness) displaying a high roughness (see below SEM images, Figure S6). For electrodeposition of PPN^+ and Co^0 and the subsequent oxidation of the cobalt particles into CoO_x, the auxiliary electrode was a platinum plate (≈ 2 cm^{-2}). A larger circular platinum grid (4 cm in diameter and 2 cm in height) was used as auxiliary electrode only for electrodeposition of Co^0 and its oxidation to CoO_x on C_{pap}, in view to facilitate the deposition process on this rough electrode. The overpotential (η) applied to the working electrode for performing water oxidation was calculated from the following equation S2:

$$\eta = E_{RHE} - 1.23\ V \qquad (S2)$$

where 1.23 V is standard potential of water oxidation reaction at pH 0.

3. Preparation of the Nanocomposite Film Modified Electrodes.

Electrosynthesis of Poly(pyrrole-alkylammonium) Film (PPN^+) Modified Electrodes. PPN^+ films were deposited either on C (also for C_{pel} and C_{pap}) or ITO electrodes, by potentiostatic oxidative electropolymerization at E_{app} = +0.95 V *vs* $Ag/AgNO_3$ for C and +1.1 V for ITO from a 4 mM solution of PN^+ in CH_3CN containing $[Bu_4N]ClO_4$ (0.1 M) as supporting electrolyte, without stirring. The polymerization of PN^+ was monitored through the anodic charge recorded during electrolysis. A full description of the procedure was previously reported by our group.[3] The anodic charge used for polymerization of PN^+ is 4, 16, 134.4 and 56 mC for C, C_{pel}, C_{pap} and ITO electrodes, respectively, which correspond to 56 mC cm^{-2}. The apparent surface coverage in ammonium units Γ_{N^+} (mol cm^{-2}), was determined by integrating the charge of the polypyrrole oxidation wave by cycling between 0.0 to +0.7 V (*vs* $Ag/AgNO_3$) at a low scan rate (10 mV s^{-1}) as previously described,[3] over an average of ten electrodes. Γ_{N^+} values ranging from 1.1 × 10^{-7} to 1.3 × 10^{-7} mol cm^{-2} were obtained for deposition of PPN^+ films onto C electrodes (surface of 0.071 cm^2, denoted C/PPN^+) using a polymerization charge of 4 mC, corresponding to an electropolymerization yield between 44 and 52%. Γ_{N^+} values ranging from 6.5 × 10^{-8} to 8.0 × 10^{-8} mol cm^{-2} were obtained for PPN^+ deposition onto ITO electrode (surface of 1.0 cm^2, denoted ITO/PPN^+) using a polymerization charge of 56 mC, corresponding to an electropolymerization yield between 26 and 32%. Γ_{N^+} values ranging from 1.50 × 10^{-7} to 1.55 × 10^{-7} mol cm^{-2} were obtained for PPN^+ deposition onto Toray carbon paper electrodes (surface of 2.4 cm^2, denoted C_{pap}/PPN^+) using a polymerization charge of 134.4 mC, corresponding to an electropolymerization yield in the range of 60.6 to 62.5%.

Electrodeposition of Metallic Cobalt Nanoparticles (Co^0) and Electrooxidation into Cobalt Oxide (CoO_x). Before the electrodeposition of cobalt, in order to have an optimum incorporation of the anionic cobalt oxalate complex ($[Co(C_2O_4)_2]^{2-}$) within the PPN^+ film, the C/PPN^+, C_{pel}/PPN^+, C_{pap}/PPN^+ and ITO/PPN^+ working electrodes were soaked during 1 h (under stirring for C, C_{pel} and C_{pap} electrodes and without stirring for ITO electrodes) in an aqueous borate buffer solution (0.1 M H_3BO_3 + 0.1 M Na_2SO_4) at pH 6 containing 4 mM

$CoSO_4$ and 20 mM $Na_2C_2O_4$, which was previously degassed under argon during 30 min.[4] The electrodeposition of Co^0 within PPN^+ films was then performed by a controlled-potential reduction of the C/PPN^+ modified electrode at E_{app} = -1.3 V *vs* Ag/AgCl (-1.3 V for C_{pel}/PPN^+ and C_{pap}/PPN^+, -1.5 V for ITO/PPN^+) in this cobalt oxalate solution under an argon atmosphere (Figure S1). Similarly to the PPN^+ electrodeposition, the charge used for cobalt electrodeposition was 4 mC for C/PPN^+, 16 mC for C_{pel}/PPN^+, 134.4 mC for C_{pap}/PPN^+ and 56 mC for ITO/PPN^+, each corresponding to 56 mC cm^{-2}. For comparative studies, an electrodeposition of Co^0 on naked C, C_{pap} and ITO electrodes was also performed following the same electrochemical procedure, but without prior soaking the electrode in the cobalt oxalate solution. Then the Co^0 nanoparticles are spontaneously oxidized into cobalt oxide (mainly CoO)[5, 6] when exposed to oxygen of air before being transferred into an aqueous borate solution (0.1 M H_3BO_3 and 0.05 M NaOH) at pH 9.2. The CoO material was then oxidized in an higher oxidation state than +II (denoted CoO_x) by 5 repeated cyclic voltammetry scans from 0 to +1.2 V *vs* Ag/AgCl (scan rate 50 mV s^{-1}) for C/PPN^+-CoO_x (Figure 2), C_{pel}/PPN^+-CoO_x and ITO/PPN^+-CoO_x and 10 repeated CV scans for C_{pap}/PPN^+-CoO_x (Figure S4) in the aforementioned aqueous solution at pH 9.2. This step does not require argon degassing. The loading of cobalt deposited on C and C_{pap} electrodes (denoted Γ_{Co}) was estimated by ICP-MS (see below).

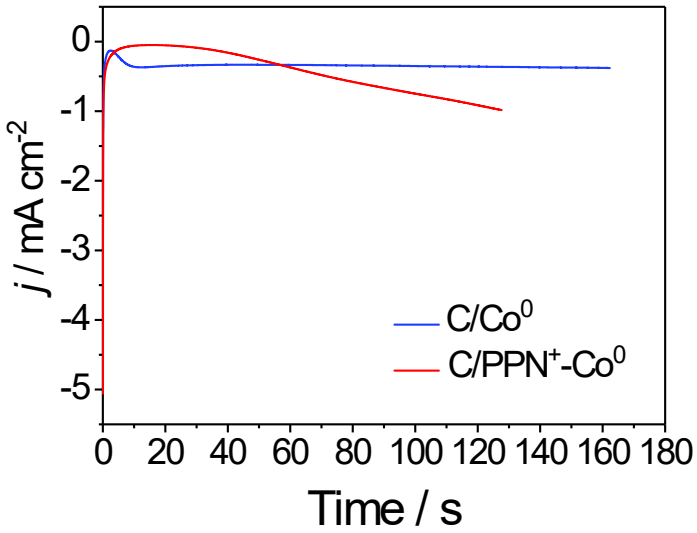

Figure S1. Cobalt deposition (E_{appl} = –1.3 V, $Q_{deposition}$ = 4 mC) on C (Γ_{Co} = 5.07 ± 0.33 × 10^{-8} mol cm^{-2}) and C/PPN^+ (Γ_{N^+} = 1.2 ± 0.1 × 10^{-7} mol cm^{-2}, Γ_{Co} = 2.27 ± 0.45 × 10^{-8} mol cm^{-2}) electrodes (3 mm of diameter) in 0.1 M borate buffer + 0.1 M $NaSO_4$ (pH 6) containing 4 mM $CoSO_4$ and 20 mM $Na_2C_2O_4$.

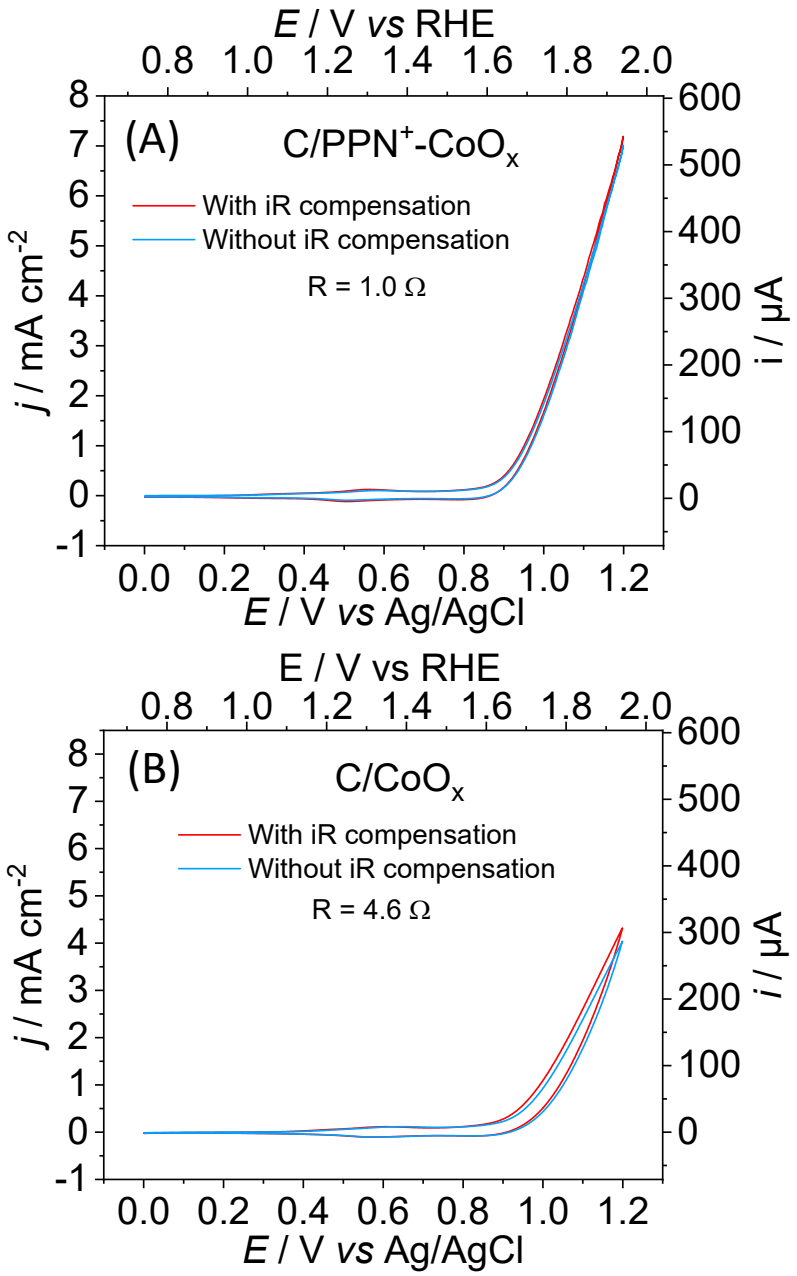

Figure S2. Cyclic voltammograms in a 0.1 M borate buffer solution (pH 9.2) recorded at (A) C/PPN$^+$-CoO_x ($\Gamma_{N^+} = 1.2 \pm 0.1 \times 10^{-7}$ mol cm^{-2}, $\Gamma_{Co} = 2.27 \pm 0.45 \times 10^{-8}$ mol cm^{-2}) and (B) C/CoO_x electrodes ($\Gamma_{Co} = 5.07 \pm 0.33 \times 10^{-8}$ mol cm^{-2}) with (red trace) or without (blue trace) iR compensation (scan rate 50 mV s^{-1}).

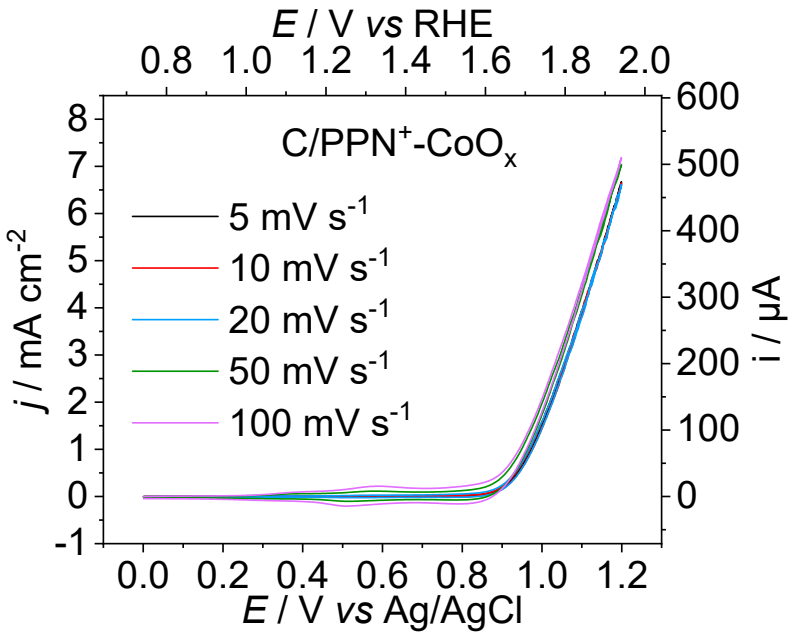

Figure S3. Cyclic voltammograms in a 0.1 M borate buffer solution (pH 9.2) recorded at C/PPN$^+$-CoO_x electrode ($\Gamma_{N^+} = 1.2 \pm 0.1 \times 10^{-7}$ mol cm^{-2}, $\Gamma_{Co} = 2.27 \pm 0.45 \times 10^{-8}$ mol cm^{-2}) with various scan rates: 5, 10, 20, 50 and 100 mV s^{-1}.

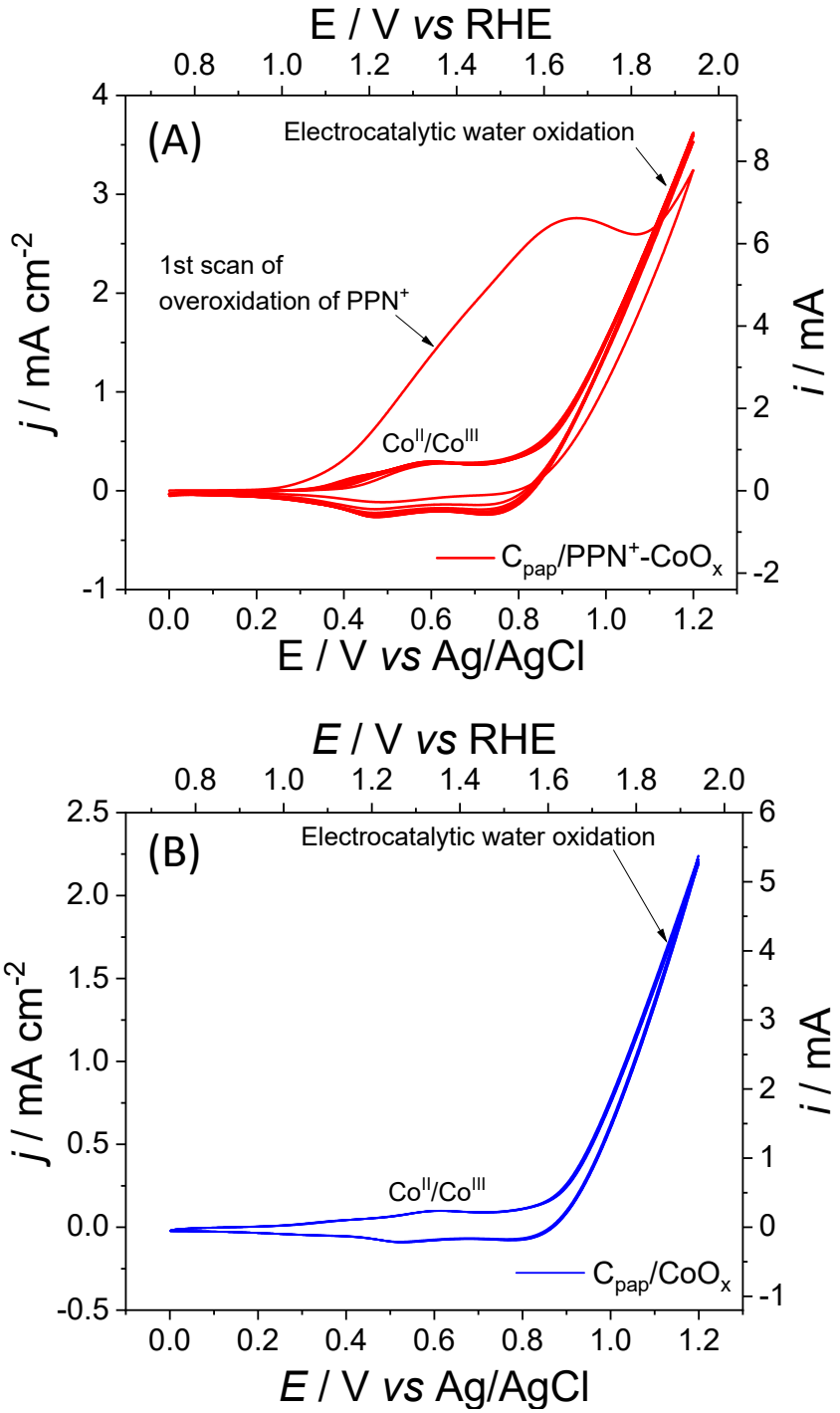

Figure S4. Electro-induced generation of CoO_x from CoO by repeated cyclic voltammetry scans (10 and 6 consecutive scans respectively in (A) and (B) ; scan rate of 50 mV s^{-1}) between 0 and + 1.2 V in a 0.1 M borate buffer solution (pH 9.2) at (A) C_{pap}/PPN^+-CoO (Γ_{N^+} = 1.53 ± 0.03 × 10^{-7} mol cm^{-2}, Γ_{Co} = 1.04 ± 0.16 × 10^{-8} mol cm^{-2}) and (B) C_{pap}/CoO electrodes (blue, Γ_{Co} = 3.70 ± 0.27 × 10^{-8} mol cm^{-2}) (2.4 cm^2).

4. Determination of Co Contents (q) on Electrode by Inductively Coupled Plasma Mass Spectrometry (ICP-MS). The amount of cobalt were determined by ICP-MS in the PPN^+-CoO_x (Γ_{N^+} = 1.2 (± 0.1) × 10^{-7} mol cm^{-2}) and CoO_x films on C electrodes (3 mm diameter), prepared with a charge of 4 mC for PPN^+ and Co^0, and in the PPN^+-CoO_x (Γ_{N^+} =

1.53 ± 0.03 × 10^{-7} mol cm^{-2}) on carbon paper electrodes (2.4 cm^2) prepared with a charge of 134.4 mC for PPN^+ and Co^0. These electrodes were first dried in air and then soaked in 5 mL of an acidic aqueous solution containing 0.45 M HNO_3. 3 h of soaking in this acidic solution is needed to entirely dissolve the PPN^+-CoO_x and CoO_x films. The complete films dissolution was then verified by cyclic voltammetry with the fully disappearance of the Co^{II}/Co^{III} redox process and the associated water oxidation catalytic wave. The cobalt concentration in the acidic solution was determined using a quadrupole ICP-MS Thermo X serie II (Thermo Electron, Bremen, Germany) equipped with an impact bead spray chamber and a standard nebulizer (0.8 mL min^{-1}). ^{59}Co isotope was selected for the measurement and ^{103}Rh isotope was used as internal standard. Polyatomic interferences were eliminated using the collision cell mode. The concentrations were obtained using an external calibration curve. Thus, the Co content (q) was estimated to be *c.a.* 1.62 ± 0.32 and 3.60 ± 0.23 nmol respectively for C/PPN^+-CoO_x and C/CoO_x electrodes which correspond respectively to Co loading of 22.75 ± 4.50 and 50.69 ± 3.30 nmol cm^{-2}. For carbon paper electrodes, the Co content in C_{pap}/PPN^+-CoO_x and C_{pap}/CoO_x was estimated to be respectively *c.a.* 24.9 ± 3.8 and 88.8 ± 6.5 nmol, which correspond respectively to a Co loading of 10.4 ± 1.6 and 37.0 ± 2.7 nmol cm^{-2}.

5. Electrochemical Impedance Spectroscopy (EIS). EIS measurements were recorded with an Autolab PGSTAT 100 potentiostat (Eco Chemie, Utrecht, The Netherlands) using the conventional three-electrode system, described above in section 2, in a 0.1 M borate buffer solution at pH 9.2. For EIS measurements, C/PPN^+-CoO_x (Γ_{N^+} = 1.2 ± 0.1 × 10^{-7} mol cm^{-2}, Γ_{Co} = 2.27 ± 0.45 × 10^{-8} mol cm^{-2}) and C/CoO_x (Γ_{Co} = 5.07 ± 0.33 × 10^{-8} mol cm^{-2}) were used and prepared on carbon electrode (3 mm of diameter). The data were recorded and operated using Nova software (version 2.1). A frequency range from 50.000 to 0.1 Hz was scanned using an amplitude of 0.02 Vrms and with a potential range between of +0.2 and +1.0 V *vs* Ag/AgCl. The ZView software was used to fit the experimental impedance data with the appropriate equivalent electrical circuit.

The complex impedance of constant phase elements (CPE) is given by

$$Z_{CPE} = \frac{1}{Q(j\omega)^n}$$

where Q is admittance constant of CPE, ω is the frequency expressed in rad/s, and n the exponent. When n=1, this is the same equation as that for the impedance of a capacitor, where Q = C.

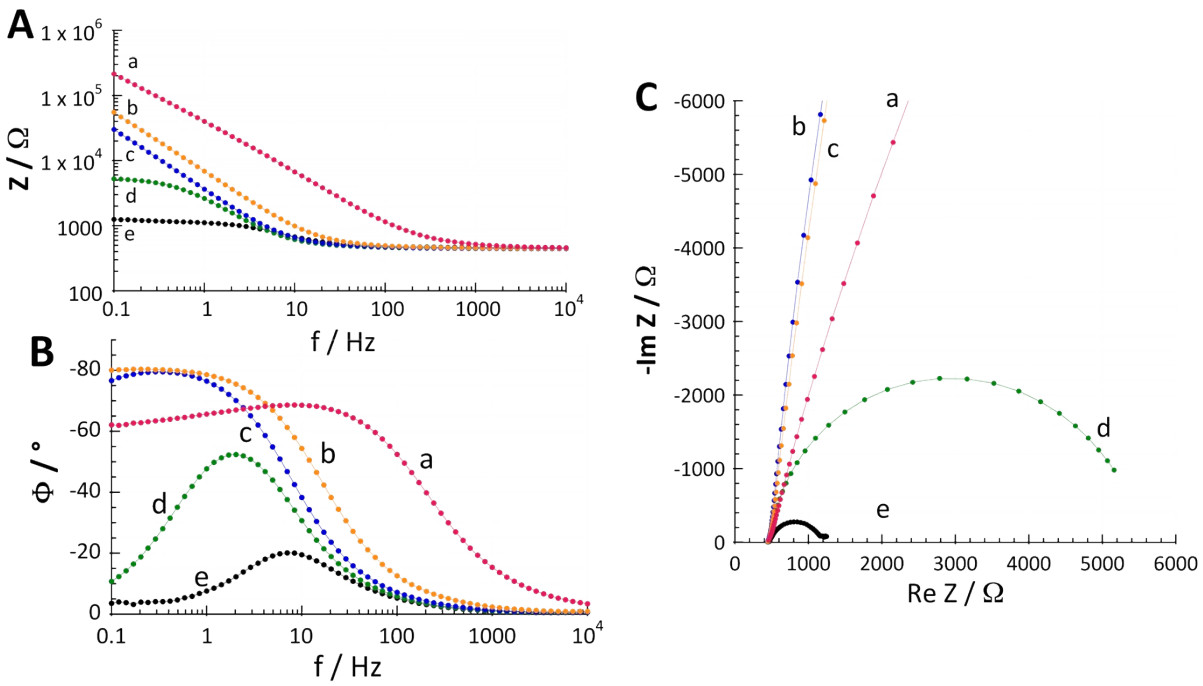

Figure S5. Bode (module (A), phase (B)) and Nyquist plots (C) recorded at the C/CoO_x (Γ_{Co} = 5.07 ± 0.33 × 10^{-8} mol cm^{-2}) electrode (3 mm of diameter) in a 0.1 M borate buffer solution (pH 9.2) at different potentials 0.2 (a), 0.6 (b), 0.8 (c), 0.9 (d) and 1.0 V (e) *vs* Ag/AgCl.

6. Calculation of Mass Activity and Turnover Frequency (TOF). The TOF value (expressed in s^{-1}) at a given overpotential is usually defined as mole of O_2 produced per second per mole of Co, O_2 produced being measured by gas chromatography. The TOF values for each Co based electrode could be also calculated from electrochemical experiments following the equation S3:

$$TOF = \frac{j \times S}{4 \times F \times n} \qquad \text{(S3)}$$

Where j is the catalytic current density (A cm^{-2}) at a given overpotential, S is the surface of the electrode (0.071 cm^2 for the carbon electrode), F is the Faraday constant (96 500 C mol^{-1}) and n is the molar number of cobalt deposited on electrode. This TOF value corresponds to its lower limit (TOF_{min}) since it was considered that all cobalt sites deposited on the electrode are active for water oxidation. The quantity of Co deposited was estimated by ICP-MS (*vide supra*).

The mass activity (expressed in A mg^{-1}) at a given overpotential is calculated from the equation S4:

$$Mass\ activity = \frac{i}{m} \qquad \text{(S4)}$$

Where i is the catalytic current at a given overpotential (A) and m is the mass of cobalt deposited on electrode (mg).

7. Tafel Plot. The Tafel curves were plotted as the overpotential (η), corrected by the ohmic potential drop ($\eta - \mathrm{iR}$, see below), in function of the current density in logarithm form following the equation S5:

$$(\eta - iR) = a + b\log\ j \qquad \text{(S5)}$$

Where j (A cm^{-2}) is the current density at a given corrected overpotential (η (V) $-$ iR) and b is the Tafel slope (V dec^{-1}). The current-overpotential data collected for Tafel plot were obtained by carring out electrolyses with C/PPN$^+$-CoO$_x$ and C/CoO$_x$ rotating disc electrodes (3 mm of diameter, with a rotation of 1200 rpm) in aqueous borate buffer solution (pH 9.2) at various potentials between +0.90 and +1.2 V *vs* Ag/AgCl, which correspond to overpotentials (η) between +0.41 V and +0.71 V (*i.e.* corresponding to corrected overpotentials $\eta - \mathrm{iR}$ between +0.41 V and +0.52 V). For each imposed potential, the current data were collected during electrolysis when the latter reaches a steady state after *c.a.* 600 s. The rotation of the electrode for the Tafel plot data collection allows reducing the mass transport effect on the catalytic current. High corrected overpotential values (above +0.52 V) were ruled out for Tafel analysis in order to avoid mass transport limitations due to a strong oxygen evolution and the ions transport into the film. In addition, low corrected overpotential values (below +0.41 V) were not considered in order to obtain relevant values of current significantly high that are not affected by background noise. As mentioned above, the η overpotentials were corrected by subtracting the ohmic potential drop (iR, where i (A) is current measured at the given overpotential and R (Ω) is the resistance measured between the reference electrode and the working electrode under rotation at 1200 rpm in aqueous borate buffer solution at pH 9.2). The R value was measured for each point of the Tafel plot (*i.e.* for each η value) and ranges between 760 and 813 Ω for C/PPN$^+$-CoO$_x$ and between 562 and 600 Ω for C/CoO$_x$. The Tafel analyses were obtained with C/PPN$^+$-CoO$_x$ ($\Gamma_{N^+} = 1.2 \pm 0.1 \times 10^{-7}$ mol cm^{-2}, $\Gamma_{Co} = 2.27 \pm 0.45 \times 10^{-8}$ mol cm^{-2}) and C/CoO$_x$ ($\Gamma_{Co} = 5.07 \pm 0.33 \times 10^{-8}$ mol cm^{-2}) electrodes that have been prepared with 4 mC of Co and PPN$^+$ as described above.

8. Atomic Force Microscopy (AFM) Observation. For electrodeposition on nonporous ITO electrodes (1.0 cm^2, 70 Ohms, from Solems), the CoO$_x$ and PPN$^+$-CoO$_x$ nanocomposite samples were prepared by using a charge of 56 mC for the deposition of Co^0 from the cobalt oxalate solution (see above the sections 2 and 3). All samples were observed with a Bruker instrument (Dimension Icon with ScanAsyst) equipped with a Bruker Stage controller and a Nanoscope® V Bruker control box. The topography images were recorded by peak force mode with different scanning ranges and a tapping nose was used for imaging. AFM cantilevers with a silicon tip on nitride lever (Bruker scanasyst-air) with a nominal spring constant of 77.6 mN m^{-1} were used. The peak force frequency and amplitude were set to 2 kHz and 150 nm, respectively. All AFM images were displayed and processed using the Gwyddion program.

9. Transmission Electron Microscopy (TEM) Observation. The PPN$^+$-CoO$_x$ and CoO$_x$ materials were separated from the ITO/PPN$^+$-CoO$_x$ and ITO/CoO$_x$ electrodes (previously prepared for AFM, see above section 9) by peeling off with a blade. The resulting powdered fragments were collected in water and a droplet of the suspension was deposited onto carbon-

coated copper grids. TEM images were recorded with a Thermo Fisher Scientific Philips CM200 instrument operating at 200 kV.

10. X-ray photoelectron spectroscopy (XPS). XPS analysis was performed with a Versa Probe II spectrometer (ULVAC-PHI) equipped with a monochromated Al Kα source (hv= 1486.6 eV). Constant pass energy of 23.3 eV was used to record the core level peaks. The fitting of the XPS spectrum was carried out with CasaXPS 2.3.15 software using Shirley background and a combination of Gaussian (70%) and Lorentzian (30%) distributions. Binding energies are referenced with respect to the adventitious carbon (C 1s BE = 284.6 eV). XPS analysis was performed on the electrode surface of C_{pel}/PPN^{+}-CoO_x (see above the section 3 for its preparation) (Figure S6).

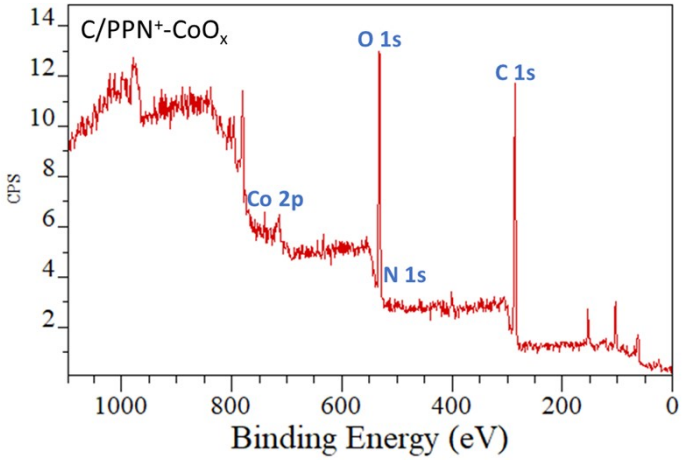

Figure S6. Survey XPS spectrum of the electrode surface of C_{pel}/PPN^{+}-CoO_x after 5 cycles between 0 to +1.2 V *vs* Ag/AgCl in 0.1 M borate buffer (pH 9.2).

11. Scanning Electron Microscopy (SEM) Observation coupled to Energy-dispersive X-Ray Spectroscopy (EDX). Secondary electron SEM images of ITO/CoO_x (Figure S7(A)) and ITO/PPN^{+}-CoO_x (Figure S7(B)) were recorded with a FEI Quanta 250 microscope equipped with a field emission gun and operating at 2 kV. SEM images and EDX spectra of C_{pap} (Figure S8) and C_{pap}/PPN^{+}-CoO_x before (Figure 8) and after (Figures 11-12) an electrolysis of 43 h at +1.2 V *vs* Ag/AgCl were recorded with a FEG Zeiss GeminiSEM500 microscope equipped with a SDD detector (EDAX OCTANE ELITE 25 with a ceramic window of Si_3N_4 – 60 mm²) for EDX.

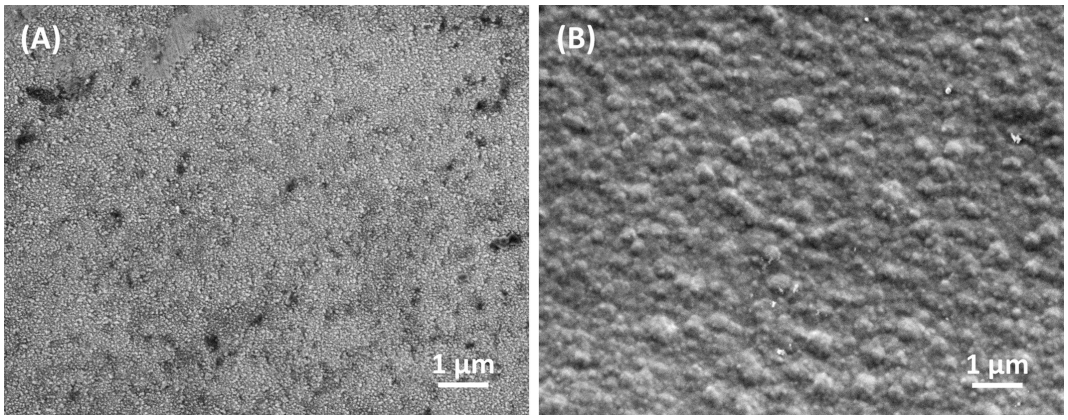

Figure S7. Secondary electron SEM images of (A) ITO/CoO_x (56 mC used for Co^0 deposition, 1 cm^{-2}), (B) ITO/PPN^+-CoO_x (56 mC used for PPN^+ and Co^0 deposition, 1 cm^{-2}).

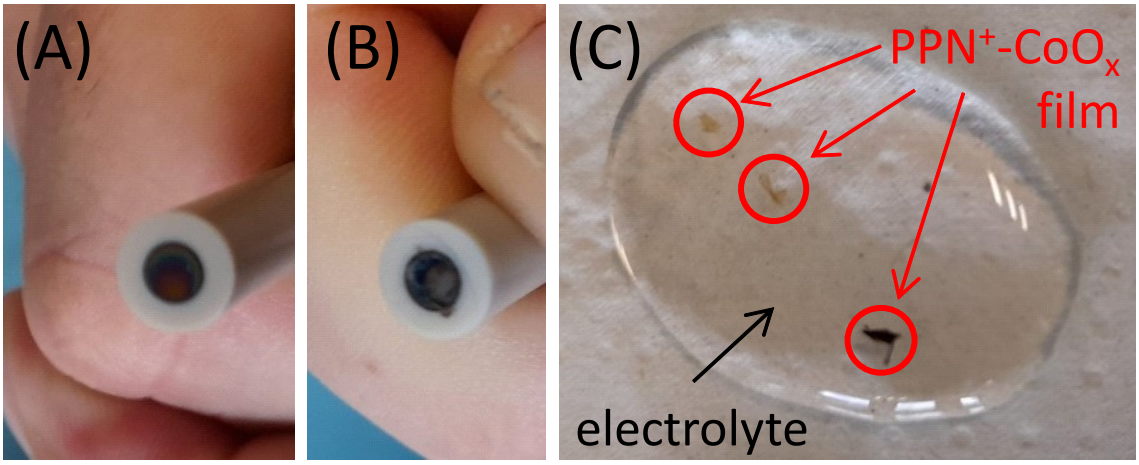

Picture S1. View of a C/PPN^+-CoO_x electrode (Γ_{N^+} = 1.2 ± 0.1 × 10^{-7} mol cm^{-2}, Γ_{Co} = 2.27 ± 0.45 × 10^{-8} mol cm^{-2}, 3 mm of diameter) (A) before and (B) after an electrolysis of 6 h at a constant potential of +1.2 V *vs* Ag/AgCl in a 0.1 M borate buffer solution (pH 9.2) under stirring. (C) View of the PPN^+-CoO_x film partially detached from the C electrode after an electrolysis of 6 h and part of the film floating in the borate buffer solution.

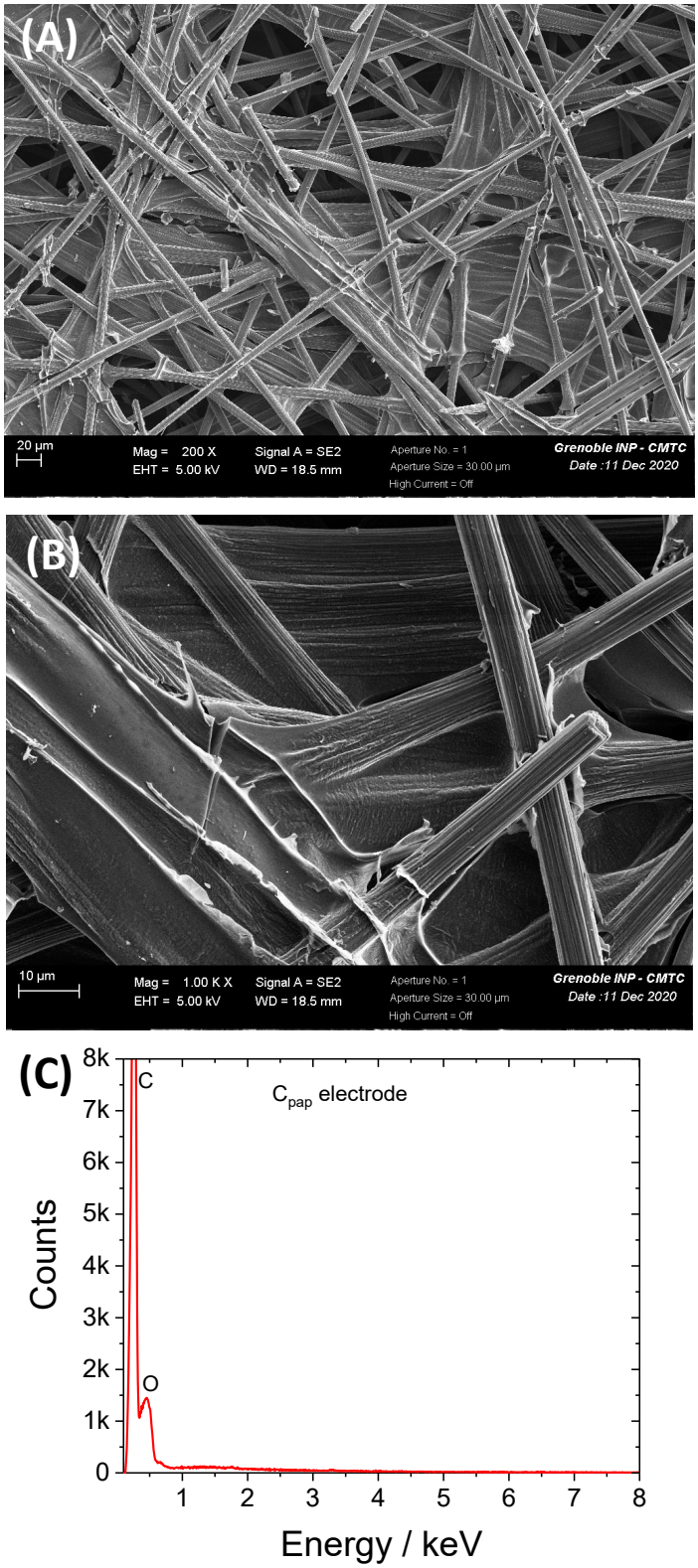

Figure S8. SEM images of C_{pap} electrode (A) 200 x magnification, (B) 1000 x magnification and (C) corresponding EDX spectrum.

12. Determination of Faradaic yield towards O_2 evolution. The Faradaic yield was determined in a home-made three-compartment cell with C_{pap}/PPN^+-CoO_x (2.4 cm^2) as working electrode, placed in the same 1st compartment with a Ag/AgCl reference and a clark electrode, and a platinum cylinder (~ 12 cm^2) as counter electrode in the 3rd compartment (see below Pictures S2-S3). The faradaic yield was calculated by measuring the quantity of oxygen evolved in the 1st compartment of the working electrode after 2h of electrolysis at 1.2 V *vs* Ag/AgCl in an aqueous borate (0.1 M) buffer at pH 9.2. The amount of oxygen evolved in the 1st compartment was determined by analysing the gas mixture in the headspace (240 mL) by gas chromatography (denoted GC, Perkin Elmer Autosystem XL, gas sampling of 100 µL, argon being the carrier gas) equipped with a 5 Å molecular sieve column (oven temperature = 303 K) and a thermal conductivity detector (TCD). The amount of O_2 dissolved in the buffer solution (60 mL) was also analysed using a Clark electrode (YSI). Prior to the electrolysis, GC/TCD and the clark electrode were calibrated by using the air (20.95 % O_2 and 78.09 % N_2) and then the initial amount of oxygen in the headspace and the buffer solution in the 1st compartment of the cell was determined. After 2h of electrolysis with a stable current of 8.4 mA (60.48 C passed), 1.52 x 10^{-4} mol of O_2 was evolved in the 1st compartment of the cell (1.42 x 10^{-4} mol in the headspace and 0.10 x 10^{-4} mol in the buffer solution). The theoretical amount of oxygen evolved (q_{theo}) for a charge of 60.48 C (Q_{exp}) is 1.57 x 10^{-4} mol, following the equation S6:

$$q_{theo} = \frac{Q_{exp}}{n_{e^-} \times F} \qquad \text{(S6)}$$

where F is the Faraday constant (96 500 C mol^{-1}) and n_{e^-} is the number of electron involved in the water oxidation which is equal to 4.Thus, the faradaic yield of water oxidation to O_2 after 2h of electrolysis is estimated to be 97 %.

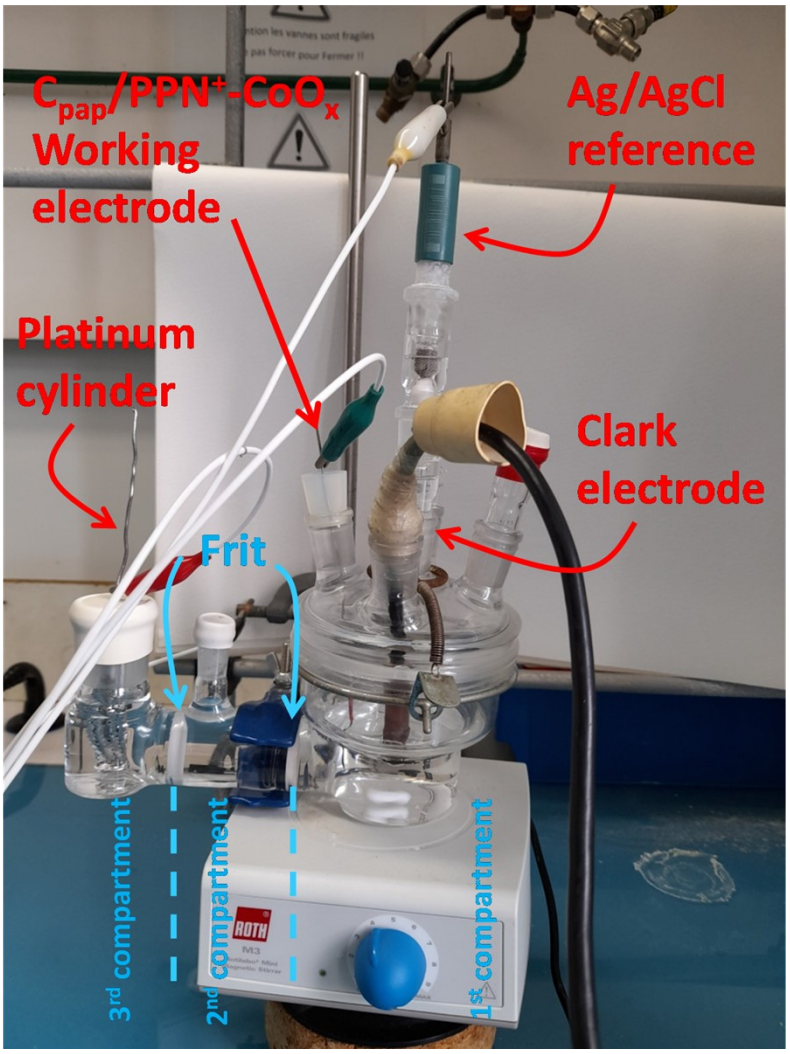

Picture S2. Three-compartment cell for the determination of faradaic yield.

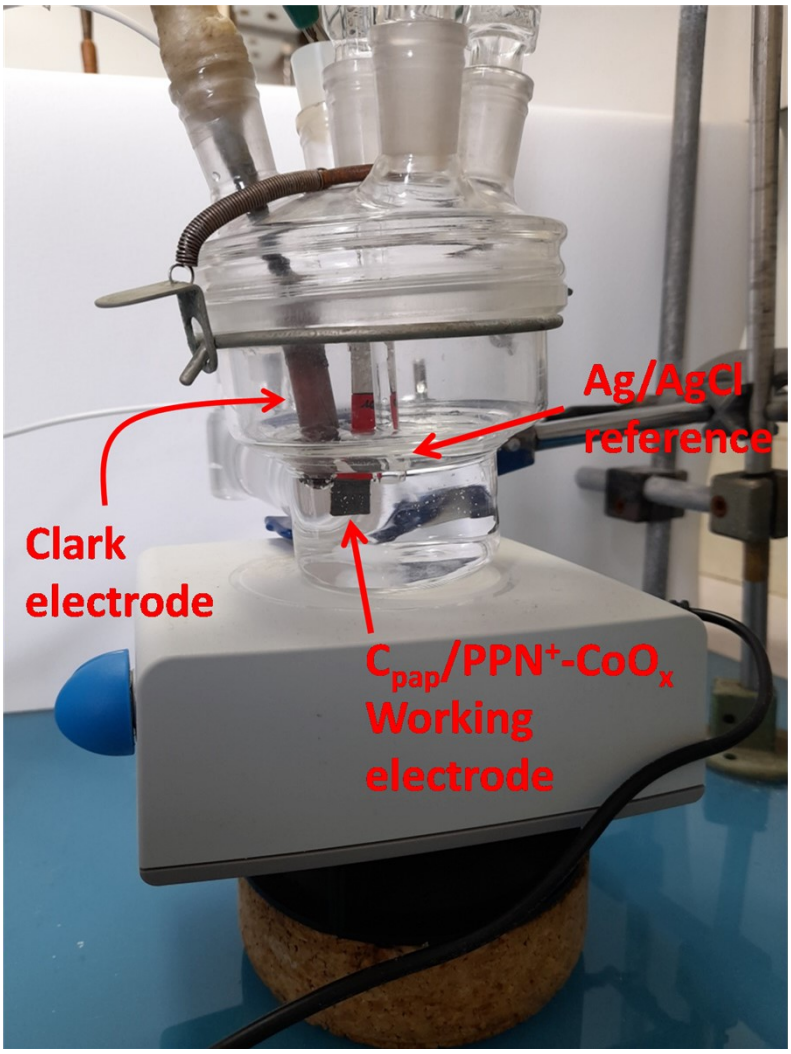

Picture S3. View of the first compartment of the three-compartment cell for the determination of faradaic yield.

REFERENCES

1. S. Cosnier, A. Deronzier, J. C. Moutet and J. F. Roland, *J. Electroanal. Chem.*, 1989, **271**, 69-81.
2. M. Zhong, T. Hisatomi, Y. Kuang, J. Zhao, M. Liu, A. Iwase, Q. Jia, H. Nishiyama, T. Minegishi, M. Nakabayashi, N. Shibata, R. Niishiro, C. Katayama, H. Shibano, M. Katayama, A. Kudo, T. Yamada and K. Domen, *J. Am. Chem. Soc.*, 2015, **137**, 5053-5060.
3. D. V. Morales, C. N. Astudillo, Y. Lattach, B. F. Urbano, E. Pereira, B. L. Rivas, J. Arnaud, J.-L. Putaux, S. Sirach, S. Cobo, J.-C. Moutet, M.-N. Collomb and J. Fortage, *Catal. Sci. Technol.*, 2018, **8**, 4030-4043.
4. A. Zouaoui, O. Stephan, A. Ourari and J. C. Moutet, *Electrochim. Acta*, 2000, **46**, 49-58.
5. D. W. Rice, P. B. P. Phipps and R. Tremoureux, *J. Electrochem. Soc.*, 1979, **126**, 1459-1466.
6. B. H. R. Suryanto, X. Lu, H. M. Chan and C. Zhao, *RSC Advances*, 2013, **3**, 20936-20942.